Materials Science & Engineering A 716 (2018) 308–315

Contents lists available at ScienceDirect

Materials Science & Engineering A

journal homepage: www.elsevier.com/locate/msea

Structure and hardness of B2 ordered refractory $AlNbTiVZr_{0.5}$ high entropy alloy after high-pressure torsion

N.D. Stepanov[a,*], N.Yu. Yurchenko[a], A.O. Gridneva[a], S.V. Zherebtsov[a], Yu.V. Ivanisenko[b], G.A. Salishchev[a]

[a] Laboratory of Bulk Nanostructured Materials, Belgorod State University, Belgorod 308015, Russia
[b] Karlsruhe Institute of Technology, Institute of Nanotechnology, Karlsruhe, Germany

ARTICLE INFO

Keywords:
High entropy alloys
High-pressure torsion
B2 phase
Laves phase
Disordering
Young's modulus

ABSTRACT

High-pressure torsion (HPT) at room temperature was applied to an $AlNbTiVZr_{0.5}$ refractory high entropy alloy. In the initial as-cast condition the alloy was composed of a coarse-grained B2 matrix phase and a continuous network of C14 Laves phase particles with the volume fraction of 19%. HPT resulted in the formation of a nanocrystalline structure in the B2 matrix with an average size of grains/subgrains of 25 nm after 5 revolutions. The B2 phase also underwent significant disordering during HPT. The Laves phase network was broken and individual particles became much thinner in comparison with those in the initial condition. Microhardness measurements have revealed typical of HPT gradient along the radius which decreased with increasing the number of revolutions. It was also found that the nanohardness of the B2 phase increased after HPT while the nanohardness of the Laves phase decreased. A strong decrease in the Young's modulus of the B2 phase was also found. Factors governing structure and properties evolution of the alloy during HPT were discussed.

1. Introduction

The so-called high entropy alloys (HEAs) attract a lot of attention from the researchers worldwide in recent years [1–4]. According to the original definition, HEAs are the alloys which composed of at least 5 elements in approximately equiatomic proportions [5]. The HEA concept provides enormous capabilities for novel alloys development for advanced applications [4,6]. Many produced HEAs have been considered as promising structural materials due to high strength, ductility, fracture and impact toughness [1,7–12]. One of the particularly attractive features of some HEAs is their high strength at elevated temperatures. For instance, HEAs composed of refractory elements (usually referred to as refractory HEAs) can have the superior specific strength to widely-used Ni-based super-alloys at temperatures up to 1000–1200 °C [13–20].

In most studies, HEAs are examined either in the as-cast condition or after heat treatment. Thermomechanical processing which can eliminate casting defects or refine the microstructure is generally used for highly ductile HEAs, which can be easily processed at room temperature [21–23]. The refractory HEAs usually possess limited ductility at low temperatures [13–20]. The only known exception is the HfNbTaTiZr alloy that can be cold-rolled to high thickness reductions at room temperature [24–27].

Processing of alloys with poor workability at low temperatures can be performed using special metal-working techniques. One of these techniques is high-pressure torsion (HPT) which is attractive due to the following capabilities: (i) processing of even brittle materials at room temperature; (ii) imposing almost unlimited strain; (iii) formation of an ultra-fine grained or even nanocrystalline structure as a result of such severe straining [28]. The application of HPT to various HEAs was already reported in some recent manuscripts [23,29–32]; however, highly-ductile alloys were used in the most studies. Processing of refractory HEAs by HPT is almost unexplored [33,34].

In the present work, we report structure and hardness of the refractory $AlNbTiVZr_{0.5}$ alloy after HPT processing. The alloy has demonstrated attractive mechanical properties both at room and elevated temperatures [35,36]. The structure of the alloy is composed of the (i) B2 ordered matrix phase and (ii) second Laves phase particles [36]. The effect of HPT on ordered structures or second phases evolution in HEAs has never been reported so far.

2. Materials and methods

The alloy with a nominal composition of $AlNbTiVZr_{0.5}$ (the subscript indicates the molar fractions of the corresponding element; if the molar fraction is unity the subscript is omitted) was produced by arc

* Correspondence to: Laboratory of Bulk Nanostructured Materials, Belgorod State University, Pobeda 85, Belgorod 308015, Russia.
E-mail addresses: stepanov@bsu.edu.ru, stepanov.nikita@icloud.com (N.D. Stepanov).

https://doi.org/10.1016/j.msea.2018.01.061
Received 18 October 2017; Received in revised form 13 January 2018; Accepted 15 January 2018

Table 1
The chemical composition of the structural constituents of the $AlNbTiVZr_{0.5}$ alloy in the initial (as-cast) condition in comparison with the actual chemical composition of the alloy.

Element, at%	Al	Nb	Ti	V	Zr
Matrix	21.1	22.8	24.8	23.0	8.3
Second phase particles	27.4	13.2	11.2	21.1	27.1
Alloy composition	23.4	21.0	22.7	21.7	11.2

melting of the elements in a low-pressure, high-purity argon atmosphere inside a water-cooled copper cavity. The purities of the alloying elements were no less than 99.9 at%. The size of the produced ingot was ~ 6 × 12 × 40 mm^3. The chemical composition of the alloy measured by energy dispersive spectroscopy (EDS) closely corresponded to the nominal chemical composition (Table 1).

For the HPT processing discs with the diameter of 10 mm and thickness of 0.8 mm were cut from the cast $AlNbTiVZr_{0.5}$ alloy ingot, then ground and mechanically polished. The discs were subjected to HPT at room temperature to 0.25, 0.5, 1, and 5 revolutions of the anvil under a pressure of 8 GPa in a Bridgman anvil-type unit with the rate of 0.5 rpm using a custom-built computer-controlled HPT device (W. Klement GmbH, Lang, Austria).

Microstructure of the $AlNbTiVZr_{0.5}$ alloy in the initial (as-cast) condition and after HPT was studied using X-ray diffraction analysis (XRD), scanning (SEM) and transmission (TEM) electron microscopy. The XRD analysis was performed using a RIGAKU diffractometer with CuKα radiation. A PowderCell software (v. 2.4) was used for the qualitative phase analysis. The obtained XRD data was also used for the calculation of a long-range order parameter (LROP) by comparing intensities of the fundamental and superlattice reflections. A detailed description of the procedure can be found elsewhere [36].

The samples for SEM observations were prepared by careful mechanical polishing. SEM back-scattered electron (BSE) images of microstructures were obtained using FEI Quanta 3D microscope equipped with an EDS detector. The actual chemical composition of the alloy was measured by EDS scanning over the area ≈ 0.5 × 0.5 mm^2. SEM examinations were carried out in a mid-thickness of a transversal section in three different characteristic areas: (i) in the central part of the disc, i.e. within ± 0.5 mm from the center; (ii) at the half of the radius, i.e. ~ 2.5 mm from the center; (iii) at the edge, i.e. ~ 4–5 mm from the center. Dimensions and the volume fraction of phases were measured by a Digimizer Image Analysis Software using SEM-BSE images.

TEM examinations were performed in a mid-thickness of the specimens in the shear plane in the vicinity (~ 1.5 mm away) of the edge. Samples for the TEM analysis were prepared by a conventional twin-jet electropolishing at a temperature of − 35 °C and an applied voltage of 29.5 V in a mixture of 600 ml of methanol, 360 ml of butanol and 60 ml of perchloric acid. The TEM investigations were performed using a JEOL JEM-2100 microscope at an accelerating voltage of 200 kV.

Both microhardness measurements and nanoindentation tests were used to study mechanical properties evolution of the $AlNbTiVZr_{0.5}$ alloy during HPT. The microhardness was measured in a transversal section in 5 different areas: in the central part of the disc and then per 1 mm away from the center. Each of the presented values represents the average of at least 10 measurements. Nanoindentation was performed in a transversal section of the specimens at the half of the radius using a Shimadzu DUH-211 s Dynamic Ultra Micro Hardness Tester with a 136-degree Vickers diamond pyramid under a 50 mN load and a speed 6.6620 mN/s applied for 5 s. Both the Vickers nanohardness and Young's modulus of constitutive phases were determined during nanoindentation. Specific attention was paid to ensure that the indents were fully located inside the desired phases and did not overlap the other one. Only accurate indention results were taken for the further consideration. The size of the indents inside the B2 and Laves phases was 2.5–3.3 μm and 1.4–2.0 μm, respectively. Each of the presented values was the average of at least 5 measurements.

3. Results

Fig. 1 shows the structure of the $AlNbTiVZr_{0.5}$ alloy in the initial (as-cast) condition. The structure was presented by coarse irregularly shaped matrix phase grains (labeled as 1 in Fig. 1a) and almost continuous chains of second phase particles (labeled as 2 in Fig. 1a) separating matrix grains. The average size of the matrix grains was ≈ 25 μm, and the average size (thickness) of the second phase particles was ≈ 2.5 μm. The volume fraction of the second phase particles was 19%. The results of the EDX analysis demonstrated that the particles were enriched with Al and Zr, and depleted of Nb and Ti (Table 1). The matrix phase had the composition close to the nominal concentrations. The results of the TEM analysis demonstrated that the matrix phase had a B2 ordered structure, while the second phase particles were a C14 (hexagonal) Laves phase (Fig. 1b).

The XRD pattern of the $AlNbTiVZr_{0.5}$ alloy in the initial (as-cast) condition (Fig. 2a) also demonstrated the presence of two phases: the B2 and C14 Laves phase. Much higher intensity of the B2 diffraction maximums was in agreement with the B2 structure of the matrix phase according to the TEM results (Fig. 1b). The XRD analysis had not revealed any noticeable changes in the phase composition of the $AlNbTiVZr_{0.5}$ alloy during HPT (Fig. 2a). The qualitative analysis demonstrated that the fractions of the B2 and Laves phases were 86.0 ± 0.3% and 14.0 ± 0.2%, respectively, in all conditions. However, the Bragg peaks belonging to both phases broadened with an increase in the revolutions numbers, most possibly due to both defects generation and

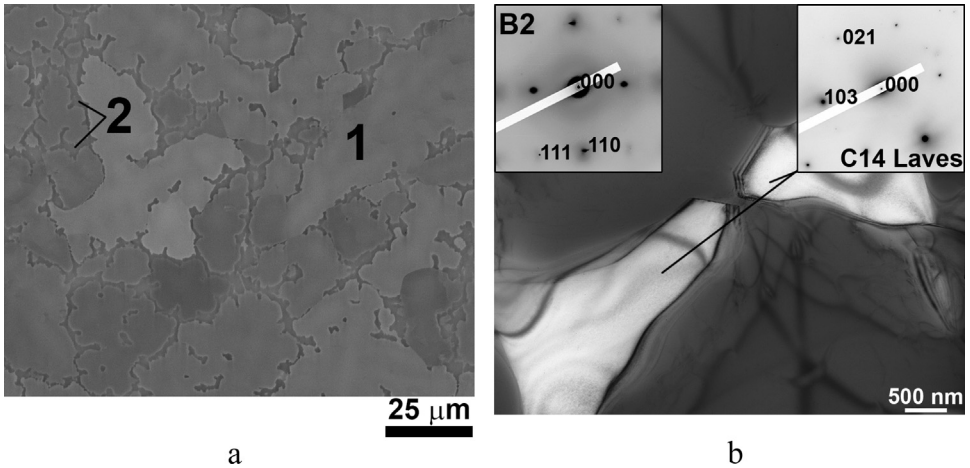

Fig. 1. Microstructure of the $AlNbTiVZr_{0.5}$ alloy in the initial (as-cast) condition, a – SEM-BSE image, b – TEM image.

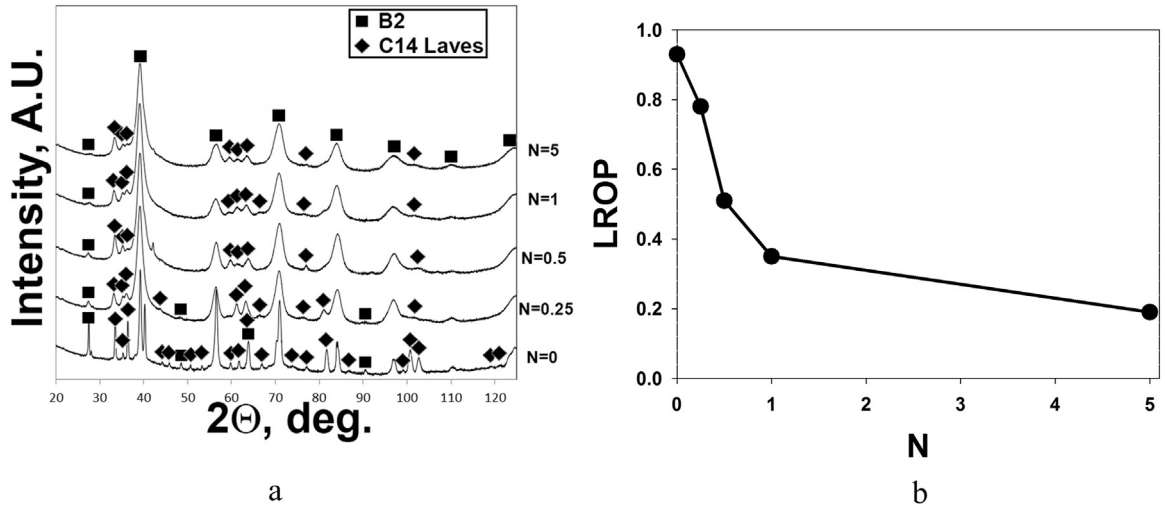

Fig. 2. Results of the XRD analysis of the AlNbTiVZr$_{0.5}$ alloy in the initial (as-cast) condition and after HPT with a different number of revolutions (N), a – XRD diffraction patters, b – long-range order parameter (LROP).

microstructure refinement during deformation. In addition, the superlattice reflections of the B2 phase obviously weakened with an increase in the number of HPT turns that can be associated with deformation-induced disordering of the B2 phase. A dependence of the long-range order parameter (LROP) on the number of revolutions (Fig. 2b) also clearly demonstrated disordering during deformation. The dependence was non-monotonic: the LROP value rapidly dropped from 0.93 in the initial condition to 0.35 after 1 revolution, and then slowly decreased to 0.19 after 5 turns.

Fig. 3 illustrates the microstructure development in the AlNbTiVZr$_{0.5}$ alloy during HPT as a function of both the number of turns and the area of examination (the center and the edge of the disc). After ¼ turns the microstructure of the alloy in the center of the disc (Fig. 3a) did not change considerably in comparison with the initial as-cast condition (Fig. 1a). With an increase in strain at the edge of the disc (Fig. 3b) more prominent changes became apparent. The continuous network of the second phase particles broke up, and some of the Laves particles became elongated owing to shear deformation. Also, observed contrast inside matrix grains suggested substructure development. After 1 revolution, the network of the Laves phase particles was broken at the center of the disc as well (Fig. 3c). Some of the particles became elongated, but many of them retained the initial shape. The shearing of the second phase particles became more pronounced with an increase in the distance from the center (Fig. 3d). Thin elongated second phase particles were observed at the edge of the specimen. However, some nearly equiaxed particles were also found. Finally, after 5 turns mostly elongated Laves particles were found in each studied part of the cross-section of the disc (Fig. 3e). At the edge a highly refined structure with thin elongated Laves particles was found (Fig. 3f). Note that both the fraction and the chemical composition of the Laves particles were quite stable during HPT that is consistent with the XRD data.

The effect of the number of revolutions on the apparent thickness of the Laves phase particles is shown in Fig. 4. Obviously, HPT resulted in a considerable flattening of the Laves phase particles. This process occurred non-monotonically with a fast decrease in the Laves phase particles thickness in the interval ¼ to 1 turn and almost stable thickness during further straining. The apparent thickness of the Laves phase particles was also strongly depended on the position: in the center of the disc the thickness was considerably greater than that at the edge. However, the difference in the thickness noticeably decreased with increasing the number of turns from 0.25 to 1. After 5 revolutions the thickness at the edge and the center of the disc was 0.4 μm and 0.6 μm, respectively.

TEM was used to investigate in details the microstructure of the matrix phase of the AlNbTiVZr$_{0.5}$ alloy after HPT (Fig. 5). After ¼ turns, a lamellar substructure with dense dislocation walls was developed (Fig. 5a). Elongated subgrains tended to align with the shear direction. After 1 whole revolution, the microstructure became highly heterogeneous (Fig. 5b); an elongated structure with high dislocation density was mainly observed. However, shear bands composed of very fine nearly equiaxed grains were also revealed. Strong azimuthal spread of selected area diffraction patters taken from these shear bands suggested the formation of a disoriented grain/subgrain structure. Besides, the diffraction pattern taken from the fine-grained bands demonstrated the absence of superlattice (i.e. (100)) reflections while clear superlattice reflections can be readily seen in the rest of the material. Finally, a relatively homogeneous structure with high density of dislocations composed of fine (average size of 25 ± 8 nm), nearly equiaxed grains/subgrains was observed after 5 HPT revolutions. After the maximum strain superlattice reflections were not observed in the selected area electron diffraction patterns.

The effect of HPT on mechanical properties of the AlNbTiVZr$_{0.5}$ alloy was evaluated by microhardness measurements (Fig. 6). In the initial as-cast condition the microhardness of the alloy was 540 HV. As expected the microhardness during HPT increased with an increase in both the number of turns and the distance from the center. The hardness increased fast when the number of rotations increased from ¼ to ½ turns and then rather weak changes were observed near the edge (3–4 mm away from the center) with increased strain. However, at the center of the disc the microhardness increased gradually with an increase in the number of turns. Even after 5 rotations, the hardness in the center was noticeably lower (620 HV) than that near the edge (4 mm away from the center - 665 HV).

The individual response of the constitutive phases (the B2 matrix and Laves phase particles) to the HPT processing was characterized using nanoindentation (Fig. 7). Both the Vickers nanohardness (Fig. 7a) and Young's modulus (Fig. 7b) evolution of the phases drastically differed from each other. Namely, HPT had opposite effects on the nanohardness of the B2 and Laves phases: the B2 matrix became harder after HPT (the nanohardness in the initial as-cast condition and after 5 HPT revolutions was 573 HV and 713 HV, respectively), while the Laves phase particles softened (976 HV and 869 HV, respectively) (Fig. 7a). In both cases, noticeable changes occurred when the number of turns increased from 0 to 1; further increase in strain had a weak effect on the nanohardness. The Young's modulus of the Laves phase did not change during HPT significantly falling in the range of 128.9–126.1 GPa (Fig. 7b). In contrast the Young's modulus of the B2 matrix gradually decreased during HPT from 128.5 GPa in the initial

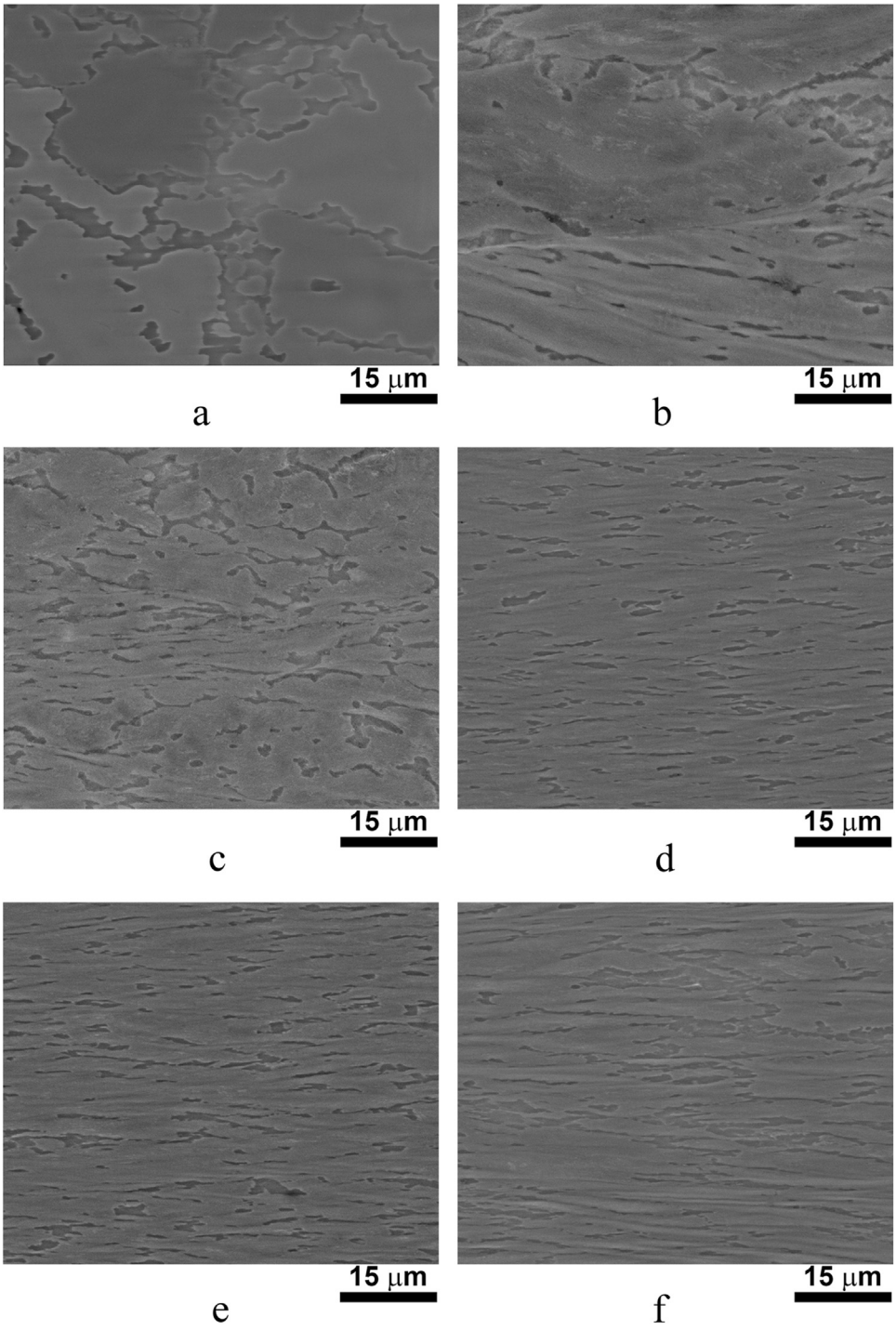

Fig. 3. SEM-BSE images of the $AlNbTiVZr_{0.5}$ alloy microstructure after HPT with different number of revolutions (N) in different areas: a, b – N = 0.25; c, d – N = 1; e, f – N = 5; a, c, e – center of the disc; b, d, f - edge of the disc.

condition to 106.7 GPa after 5 revolutions.

4. Discussion

In the present work, the effect of HPT on the structure and mechanical properties of the refractory $AlNbTiVZr_{0.5}$ HEA was studied. In the initial as-cast condition the alloy was composed of the B2 matrix phase and the Laves phase particles which formed a continuous network (Fig. 1). Although the structure and mechanical properties of HEAs after HPT were rather extensively studied, the majority of the examined alloys had simpler structures mostly consisted of a single random fcc or bcc solid solutions [23,29,33,34,37,38]. Therefore some aspects of the behavior demonstrated by $AlNbTiVZr_{0.5}$ alloy have never been considered so far.

Two major effects of HPT on the B2 matrix phase structure of the $AlNbTiVZr_{0.5}$ alloy were observed: (i) significant microstructure refinement with the formation of nano-sized grains/subgrains with an average size of 25 nm (Fig. 5c); (ii) pronounced decrease in the LROP value (Fig. 2b). HPT is known to be an effective tool for microstructure refinement of various materials, including hard-to-deform ones [28]. A number of works [28,39–42] reported the effect of HPT on ordered, intermetallic-based alloys including those with the B2 structure. A common point for both disordered alloys and ordered alloys/intermetallic compounds was a possibility to produce very fine (even nanocrystalline) grains using HPT. The grain size attained in the present study is also comparable to that reported for other refractory HEAs with

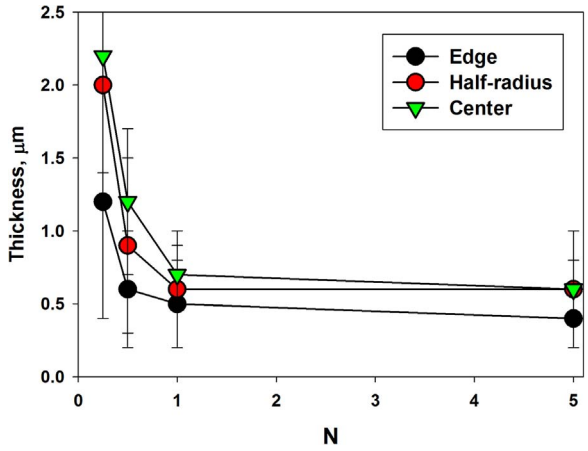

Fig. 4. The apparent thickness of the Laves phase particles in the $AlNbTiVZr_{0.5}$ alloy depending on the number of HPT revolutions (N) in different areas.

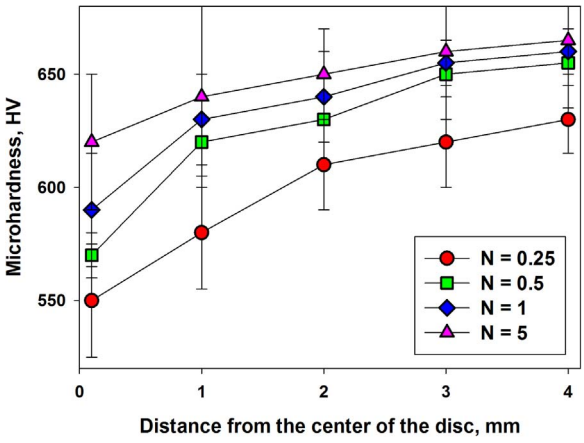

Fig. 6. Dependence of the microhardness of the $AlNbTiVZr_{0.5}$ alloy on the distance from the center of the disc after different numbers of revolutions (N).

a disordered bcc structure like HfNbTaTiZr or AlNbTiV (≈ 50 nm [33,34]).

Although disordering of initially ordered alloys due to HPT is also well-known, this phenomenon has never been reported for HEAs. The result of the present work suggests rather similar behavior between HEAs and "usual" ordered alloys, however somewhat faster kinetics of the disordering can be noted in the former case. For example, the LROP in Ni_3Al sharply decreased with an increase in the number of revolutions from 0 to 2, and afterward did not change [39]. In our case the $AlNbTiVZr_{0.5}$ alloy reached the saturation stage already after the first revolution (Fig. 2b). This is probably due to a not perfectly ordered structure (LROP equaled to 0.93) of the initial multicomponent B2 phase of the $AlNbTiVZr_{0.5}$ alloy (Table 1), where atoms of the one species most probably can occupy the different sites of the lattice [4]. The TEM images can also suggest rather heterogeneous character of the disordering: the superlattice reflections first disappeared in the alloy inside the shear bands (Fig. 5b). Further microstructure evolution in the alloy was associated with the propagation of the shear bands and involvement of the major part of the specimen into deformation thereby decreasing the LROP. A similar phenomenon was earlier reported for the $L1_2$ compounds like Cu_3Al and Ni_3Al [43,44] deformed by HPT. Local disordering in bands (or veins) of in $L1_2$ compounds was proposed to be a prerequisite for the nanostructure formation due to increased dislocation mobility in the disordered structure. The inhomogeneity of

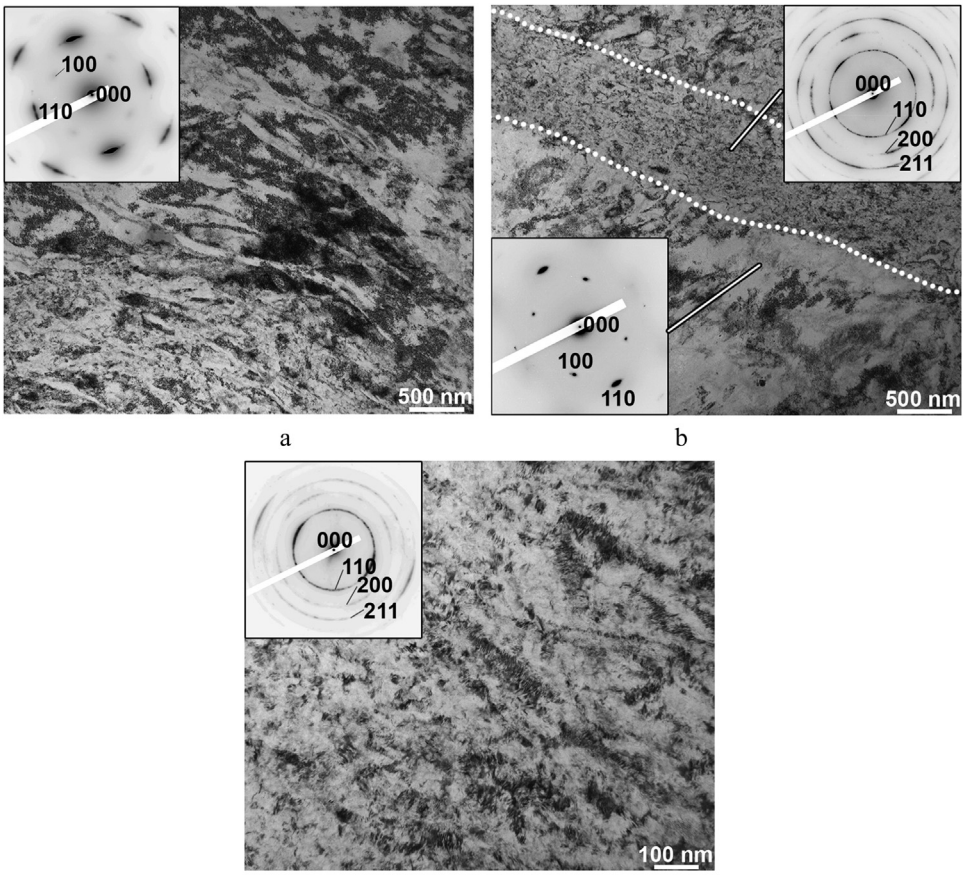

Fig. 5. TEM bright-field images of the $AlNbTiVZr_{0.5}$ alloy microstructure after HPT: a – 0.25 turns; b – 1 turn; c – 5 turns.

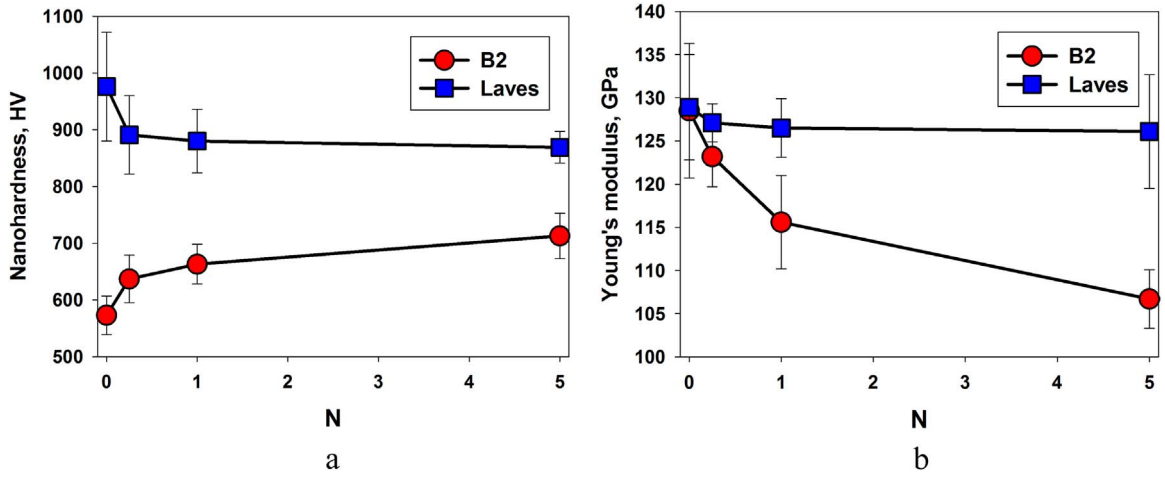

Fig. 7. Dependences of the (a) nanohardness and (b) Young's modulus of the constitutive phases of the $AlNbTiVZr_{0.5}$ alloy after HPT on the number of revolutions (N).

the disordering process in the studied $AlNbTiVZr_{0.5}$ alloy can be the reason why local TEM investigations discovered only disordered bcc phase after 5 revolutions (Fig. 5c) while the XRD pattern taken over much larger area still demonstrated weak superlattice B2 reflection (Fig. 2a).

HPT also significantly affected the Laves phase particles in the $AlNbTiVZr_{0.5}$ alloy. The initial continuous network of the Laves phase was broken at the initial stages of deformation and then the individual particles underwent significant flattening; the development of both processes resulted in an elongated shape of the Laves phase particles (Figs. 3 and 4). The Laves phase particles morphology changed heterogeneously due to an apparent effect of an imposed strain gradient along the section of the disc [28]. Most likely, the development of the shear bands in the B2 matrix intensified also the fragmentation and flattening of the Laves phase particles.

It should be noted, that some decrease in the thickness of the Laves phase particles can be associated with a stereological factor. A two-dimensional section does not give the true thickness of a lamella lying at an arbitrary angle to the plane of such a section [45,46]. At small strains this angle may be quite large, and the apparent thickness is, therefore, large as well. On the other hand, large strains tend to rotate the lamellae to coincidence with a plane normal to the compression axis (Fig. 3d–f). In such instances the lamellae are close to normal to the section plane, and an axial section does yield a reasonable approximation of the actual platelet thickness.

The presented SEM images (Fig. 3) suggested good strain compatibility between both phases since no signs of cracks/voids were observed at the interphases. This is not surprising since the Young's moduli values of both phases in the initial as-cast condition were very similar to each other (Fig. 7b). In addition, no changes in fractions or chemical compositions of the phases after HPT were found (Figs. 2a and 4). In many alloys, HPT resulted in phase transformations like dissolution/precipitation of second phases [47,48]. Possibly, suggested "sluggish" diffusion in HEAs [3] makes the structure of the $AlNbTiVZr_{0.5}$ alloy more stable, however there is no published experimental proves on slower diffusion in refractory HEAs.

Mechanical properties of the $AlNbTiVZr_{0.5}$ alloy were also significantly affected by HPT. The microhardness measurements have revealed typical dependencies: hardness increased with the number of turns until saturation was reached; strengthening occurred much faster at the edge of the disc than in the center (Fig. 7). The latter is associated with the well-known strain gradient along the radii of the HPT-processing discs [28].

The hardening of the alloy is attributed to an increase in hardness of the B2 phase (Fig. 7a) in accordance with the Hall-Petch relationship due to significant microstructure refinement (Fig. 5). On the other hand disordering (Fig. 2b) can result in some softening of the B2 phase [49]. Probably, the competition between grain boundary strengthening and softening due to disordering is responsible for the weak growth of the nanohardness values of the B2 phase in the interval from 1 to 5 HPT revolutions (Fig. 7a) in spite of considerable refinement of the structure (compare Fig. 5b and c).

The observed decrease in the Young's modulus of the B2 phase (Fig. 7b) can also be associated with disordering of the B2 phase (Fig. 2b). This suggestion is in agreement with the results reported in [50,51] where a decrease in the Young's modulus of ordered compounds like the $L1_2$ phase was ascribed to a decrease in the LROP. In addition, it is well established that HPT produces a strong simple shear texture in metals and alloys [52,53]. Changes in texture can also contribute to mechanical properties including elastic modulus of the B2 phase after HPT [54,55].

In turn, the Laves phase particles become softer after HPT (Fig. 7a). Although softening of pure metals and alloys during HPT has been already reported [56,57], the reasons why the Laves phase particles softened after HPT of the $AlNbTiVZr_{0.5}$ alloy are unclear at the moment and require additional studies.

5. Conclusions

In the present work, the evolution of microstructure and mechanical properties of the $AlNbTiVZr_{0.5}$ refractory high entropy alloy was studied. Following conclusions were drawn.

1) The $AlNbTiVZr_{0.5}$ alloy produced by arc melting was composed of coarse grains of the B2 ordered matrix phase separated by a network of the C14 Laves phase particles. The Laves phase particles were enriched with Al and Zr and depleted of Ti.
2) The HPT processing resulted in refinement of the as-cast structure of the $AlNbTiVZr_{0.5}$ alloy. For instance, the average size of grains/subgrains of the B2 matrix after 5 turns was 25 nm. The formation of the nanocrystalline structure was primarily attributed to shear banding. The network of the Laves phase was broken and the individual particles become much thinner in comparison with the initial condition. In addition to microstructure refinement, pronounced disordering of the B2 phase occurred. Disordering progressed locally and was associated with propagation of shear bands.
3) The microhardness of the $AlNbTiVZr_{0.5}$ alloy increased from 550 HV to maximum of 665 HV after 5 HPT rotations. Measurements of the nanohardness of individual phases had revealed that the hardness increased due to structure refinement of the B2 phase while the Laves phase became softer during HPT. A pronounced decrease in the Young's modulus of the B2 phase from 128.5 GPa in the initial

condition to 106.7 GPa after 5 rotations was found. The change of the elastic modulus was primarily attributed to disordering of the B2 phase.

Acknowledgements

The authors gratefully acknowledge the financial support from the Russian Science Foundation Grant No. 14-19-01104. The authors are grateful to the personnel of the Joint Research Center, «Technology and Materials», Belgorod State University, for their assistance with the instrumental analysis. The authors are also grateful to Dr. M.A. Tikhonovsky for supplying the ingot of the investigated alloy.

References

[1] Y. Zhang, T.T. Zuo, Z. Tang, M.C. Gao, K.A. Dahmen, P.K. Liaw, Z.P. Lu, Microstructures and properties of high-entropy alloys, Prog. Mater. Sci. 61 (2014), http://dx.doi.org/10.1016/j.pmatsci.2013.10.001.

[2] E.J. Pickering, N.G. Jones, High-entropy alloys: a critical assessment of their founding principles and future prospects, Int. Mater. Rev. (2016) 183–202, http://dx.doi.org/10.1080/09506608.2016.1180020.

[3] M.-H. Tsai, J.-W. Yeh, High-entropy alloys: a critical review, Mater. Res. Lett. 2 (2014) 107–123, http://dx.doi.org/10.1080/21663831.2014.912690.

[4] D.B. Miracle, O.N. Senkov, A critical review of high entropy alloys and related concepts, Acta Mater. 122 (2017) 448–511, http://dx.doi.org/10.1016/j.actamat.2016.08.081.

[5] J.-W. Yeh, S.-K. Chen, S.-J. Lin, J.-Y. Gan, T.-S. Chin, T.-T. Shun, C.-H. Tsau, S.-Y. Chang, Nanostructured high-entropy alloys with multiple principal elements: novel alloy design concepts and outcomes, Adv. Eng. Mater. 6 (2004) 299–303, http://dx.doi.org/10.1002/adem.200300567.

[6] D. Miracle, J. Miller, O. Senkov, C. Woodward, M. Uchic, J. Tiley, Exploration and development of high entropy alloys for structural applications, Entropy 16 (2014) 494–525, http://dx.doi.org/10.3390/e16010494.

[7] F. Otto, A. Dlouhý, C. Somsen, H. Bei, G. Eggeler, E.P. George, The influences of temperature and microstructure on the tensile properties of a CoCrFeMnNi high-entropy alloy, Acta Mater. 61 (2013) 5743–5755, http://dx.doi.org/10.1016/j.actamat.2013.06.018.

[8] Z. Li, K.G. Pradeep, Y. Deng, D. Raabe, C.C. Tasan, Metastable high-entropy dual-phase alloys overcome the strength–ductility trade-off, Nature 534 (2016) 227–230, http://dx.doi.org/10.1038/nature17981.

[9] B. Gludovatz, A. Hohenwarter, K.V.S. Thurston, H. Bei, Z. Wu, E.P. George, R.O. Ritchie, Exceptional damage-tolerance of a medium-entropy alloy CrCoNi at cryogenic temperatures, Nat. Commun. (2016) 10602, http://dx.doi.org/10.1038/ncomms10602.

[10] B. Gludovatz, A. Hohenwarter, D. Catoor, E.H. Chang, E.P. George, R.O. Ritchie, A fracture-resistant high-entropy alloy for cryogenic applications, Science 345 (6201) (2014) 1153–1158, http://dx.doi.org/10.1126/science.1254581 (80-.).

[11] Z. Li, C.C. Tasan, H. Springer, B. Gault, D. Raabe, Interstitial atoms enable joint twinning and transformation induced plasticity in strong and ductile high-entropy alloys, Sci. Rep. 7 (2017) 40704, http://dx.doi.org/10.1038/srep40704.

[12] D. Li, Y. Zhang, The ultrahigh charpy impact toughness of forged AlxCoCrFeNi high entropy alloys at room and cryogenic temperatures, Intermetallics 70 (2016) 24–28, http://dx.doi.org/10.1016/j.intermet.2015.11.002.

[13] O.N. Senkov, G.B. Wilks, D.B. Miracle, C.P. Chuang, P.K. Liaw, Refractory high-entropy alloys, Intermetallics 18 (2010) 1758–1765, http://dx.doi.org/10.1016/j.intermet.2010.05.014.

[14] O.N. Senkov, S.V. Senkova, C.F. Woodward, Effect of aluminum on the microstructure and properties of two refractory high-entropy alloys, Acta Mater. 68 (2014) 214–228, http://dx.doi.org/10.1016/j.actamat.2014.01.029.

[15] O.N. Senkov, S.V. Senkova, C. Woodward, D.B. Miracle, Low-density, refractory multi-principal element alloys of the Cr–Nb–Ti–V–Zr system: microstructure and phase analysis, Acta Mater. 61 (2013) 1545–1557, http://dx.doi.org/10.1016/j.actamat.2012.11.032.

[16] O.N. Senkov, S.V. Senkova, D.B. Miracle, C. Woodward, Mechanical properties of low-density, refractory multi-principal element alloys of the Cr–Nb–Ti–V–Zr system, Mater. Sci. Eng. A 565 (2013) 51–62, http://dx.doi.org/10.1016/j.msea.2012.12.018.

[17] O.N. Senkov, C. Woodward, D.B. Miracle, Microstructure and properties of aluminum-containing refractory high-entropy alloys, JOM 66 (2014) 2030–2042, http://dx.doi.org/10.1007/s11837-014-1066-0.

[18] N.D. Stepanov, N.Y. Yurchenko, D.V. Skibin, M.A. Tikhonovsky, G.A. Salishchev, Structure and mechanical properties of the AlCrxNbTiV (x = 0, 0.5, 1, 1.5) high entropy alloys, J. Alloy. Compd. 652 (2015) 266–280, http://dx.doi.org/10.1016/j.jallcom.2015.08.224.

[19] N.Y. Yurchenko, N.D. Stepanov, D.G. Shaysultanov, M.A. Tikhonovsky, G.A. Salishchev, Effect of Al content on structure and mechanical properties of the AlxCrNbTiVZr (x??=??0; 0.25; 0.5; 1) high-entropy alloys, Mater. Charact. 121 (2016) 125–134, http://dx.doi.org/10.1016/j.matchar.2016.09.039.

[20] N.D. Stepanov, D.G. Shaysultanov, G.A. Salishchev, M.A. Tikhonovsky, Structure and mechanical properties of a light-weight AlNbTiV high entropy alloy, Mater. Lett. 142 (2015) 153–155, http://dx.doi.org/10.1016/j.matlet.2014.11.162.

[21] N. Stepanov, M. Tikhonovsky, N. Yurchenko, D. Zyabkin, M. Klimova, S. Zherebtsov, A. Efimov, G. Salishchev, Effect of cryo-deformation on structure and properties of CoCrFeNiMn high-entropy alloy, Intermetallics 59 (2015) 8–17, http://dx.doi.org/10.1016/j.intermet.2014.12.004.

[22] N.D. Stepanov, D.G. Shaysultanov, R.S. Chernichenko, N.Y. Yurchenko, S.V. Zherebtsov, M.A. Tikhonovsky, G.A. Salishchev, Effect of thermomechanical processing on microstructure and mechanical properties of the carbon-containing CoCrFeNiMn high entropy alloy, J. Alloy. Compd. 693 (2017) 394–405, http://dx.doi.org/10.1016/j.jallcom.2016.09.208.

[23] B. Schuh, F. Mendez-Martin, B. Völker, E.P.P. George, H. Clemens, R. Pippan, A. Hohenwarter, B. V??lker, E.P.P. George, H. Clemens, R. Pippan, A. Hohenwarter, Mechanical properties, microstructure and thermal stability of a nanocrystalline CoCrFeMnNi high-entropy alloy after severe plastic deformation, Acta Mater. 96 (2015) 258–268, http://dx.doi.org/10.1016/j.actamat.2015.06.025.

[24] O.N. Senkov, S.L. Semiatin, Microstructure and properties of a refractory high-entropy alloy after cold working, J. Alloy. Compd. 649 (2015) 1110–1123, http://dx.doi.org/10.1016/j.jallcom.2015.07.209.

[25] O.N. Senkov, J.M. Scott, S.V. Senkova, D.B. Miracle, C.F. Woodward, Microstructure and room temperature properties of a high-entropy TaNbHfZrTi alloy, J. Alloy. Compd. 509 (2011) 6043–6048, http://dx.doi.org/10.1016/j.jallcom.2011.02.171.

[26] O.N. Senkov, J.M. Scott, S.V. Senkova, F. Meisenkothen, D.B. Miracle, C.F. Woodward, Microstructure and elevated temperature properties of a refractory TaNbHfZrTi alloy, J. Mater. Sci. 47 (2012) 4062–4074, http://dx.doi.org/10.1007/s10853-012-6260-2.

[27] W. Wu, S. Ni, Y. Liu, M. Song, Effects of cold rolling and subsequent annealing on the microstructure of a HfNbTaTiZr high-entropy alloy, J. Mater. Res. 31 (2016) 3815–3823, http://dx.doi.org/10.1557/jmr.2016.445.

[28] A.P. Zhilyaev, T.G. Langdon, Using high-pressure torsion for metal processing: fundamentals and applications, Prog. Mater. Sci. 53 (2008) 893–979, http://dx.doi.org/10.1016/j.pmatsci.2008.03.002.

[29] D.-H. Lee, I.-C. Choi, M.-Y. Seok, J. He, Z. Lu, J.-Y. Suh, M. Kawasaki, T.G. Langdon, J. Jang, Nanomechanical behavior and structural stability of a nanocrystalline CoCrFeNiMn high-entropy alloy processed by high-pressure torsion, J. Mater. Res. 30 (2015) 2804–2815, http://dx.doi.org/10.1557/jmr.2015.239.

[30] Q. Tang, Y. Huang, H. Cheng, X. Liao, T.G. Langdon, P. Dai, The effect of grain size on the annealing-induced phase transformation in an Al0.3CoCrFeNi high entropy alloy, Mater. Des. 105 (2016) 381–385, http://dx.doi.org/10.1016/j.matdes.2016.05.079.

[31] Q.H. Tang, Y.Y. Huang, Y.Y. Huang, X.Z. Liao, T.G. Langdon, P.Q. Dai, Hardening of an Al0.3CoCrFeNi high entropy alloy via high-pressure torsion and thermal annealing, Mater. Lett. 151 (2015) 126–129, http://dx.doi.org/10.1016/j.matlet.2015.03.066.

[32] A. Heczel, M. Kawasaki, J.L. Lábár, J. Jang, T.G. Langdon, J. Gubicza, Defect structure and hardness in nanocrystalline CoCrFeMnNi high-entropy alloy processed by high-pressure torsion, J. Alloy. Compd. 711 (2017) 143–154, http://dx.doi.org/10.1016/j.jallcom.2017.03.352.

[33] B. Schuh, B. Völker, V. Maier-Kiener, J. Todt, J. Li, A. Hohenwarter, Phase Decomposition of a single-phase AlTiVNb high-entropy alloy after severe plastic deformation and annealing, Adv. Eng. Mater. (2017) 1600674, http://dx.doi.org/10.1002/adem.201600674.

[34] B. Schuh, B. Völker, J. Todt, N. Schell, L. Perriere, J. Li, J.P. Couzinié, A. Hohenwarter, Thermodynamic instability of a nanocrystalline, single-phase TiZrNbHfTa alloy and its impact on the mechanical properties, Acta Mater. 142 (2017) 201–212, http://dx.doi.org/10.1016/j.actamat.2017.09.035.

[35] N.D.D. Stepanov, N.Y.Y. Yurchenko, V.S.S. Sokolovsky, M.A.A. Tikhonovsky, G.A.A. Salishchev, An AlNbTiVZr0.5 high-entropy alloy combining high specific strength and good ductility, Mater. Lett. 161 (2015) 136–139, http://dx.doi.org/10.1016/j.matlet.2015.08.099.

[36] N.Y. Yurchenko, N.D. Stepanov, S.V. Zherebtsov, M.A. Tikhonovsky, G.A. Salishchev, Structure and mechanical properties of B2 ordered refractory AlNbTiVZrx (x = 0–1.5) high-entropy alloys, Mater. Sci. Eng. A 704 (2017) 82–90, http://dx.doi.org/10.1016/j.msea.2017.08.019.

[37] H. Shahmir, J. He, Z. Lu, M. Kawasaki, T.G. Langdon, Evidence for superplasticity in a CoCrFeNiMn high-entropy alloy processed by high-pressure torsion, Mater. Sci. Eng. A 685 (2017) 342–348, http://dx.doi.org/10.1016/j.msea.2017.01.016.

[38] P.F. Yu, H. Cheng, L.J. Zhang, H. Zhang, Q. Jing, M.Z. Ma, P.K. Liaw, G. Li, R.P. Liu, Effects of high pressure torsion on microstructures and properties of an Al0.1CoCrFeNi high-entropy alloy, Mater. Sci. Eng. A 655 (2016) 283–291, http://dx.doi.org/10.1016/j.msea.2015.12.085.

[39] A.V. Korznikov, G. Tram, O. Dimitrov, G.F. Korznikova, S.R. Idrisova, Z. Pakiela, Mechanism of nanocrystalline structure formation in Ni3Al during severe plastic deformation, Acta Mater. 49 (2001) 663–671, http://dx.doi.org/10.1016/S1359-6454(00)00345-1.

[40] D.G. Morris, M.A. Muñoz-Morris, Microstructural refinement in alloys and intermetallics by severe plastic deformation, J. Alloys Compd. 185 (S1) (2012) S180–S185, http://dx.doi.org/10.1016/j.jallcom.2011.10.069.

[41] D. Geist, C. Gammer, C. Rentenberger, H.P. Karnthaler, Sessile dislocations by reactions in NiAl severely deformed at room temperature, J. Alloy. Compd. 621 (2015) 371–377, http://dx.doi.org/10.1016/j.jallcom.2014.09.226.

[42] C. Mangler, C. Gammer, H.P. Karnthaler, C. Rentenberger, Structural modifications during heating of bulk nanocrystalline FeAl produced by high-pressure torsion, Acta Mater. 58 (2010) 5631–5638, http://dx.doi.org/10.1016/j.actamat.2010.06.036.

[43] C. Rentenberger, H.P. Karnthaler, On the evolution of a deformation induced nanostructure in a Ni_3Al alloy, Acta Mater. 53 (2005) 3031–3040, http://dx.doi.org/10.1016/j.actamat.2005.03.016.

[44] C. Rentenberger, H.P. Karnthaler, Extensive disordering in long-range-ordered Cu_3Au induced by severe plastic deformation studied by transmission electron microscopy, Acta Mater. 56 (2008) 2526–2530, http://dx.doi.org/10.1016/j.actamat.2008.01.035.

[45] H.J.G. Gundersen, T.B. Jensen, R. ØSterby, Distribution of membrane thickness determined by lineal analysis, J. Microsc. 113 (1978) 27–43, http://dx.doi.org/10.1111/j.1365-2818.1978.tb00091.x.

[46] S. Mironov, M. Murzinova, S. Zherebtsov, G.A. Salishchev, S.L. Semiatin, Microstructure evolution during warm working of Ti-6Al-4V with a colony-α microstructure, Acta Mater. 57 (2009) 2470–2481, http://dx.doi.org/10.1016/j.actamat.2009.02.016.

[47] B.B. Straumal, B. Baretzky, A.A. Mazilkin, F. Phillipp, O.A. Kogtenkova, M.N. Volkov, R.Z. Valiev, Formation of nanograined structure and decomposition of supersaturated solid solution during high pressure torsion of Al-Zn and Al-Mg alloys, Acta Mater. 52 (2004) 4469–4478, http://dx.doi.org/10.1016/j.actamat.2004.06.006.

[48] B. Straumal, A. Korneva, P. Zieba, Phase transitions in metallic alloys driven by the high pressure torsion, Arch. Civ. Mech. Eng. 14 (2014) 242–249, http://dx.doi.org/10.1016/j.acme.2013.07.002.

[49] V.N. Lipatnikov, A.A. Rempel, A.I. Gusev, Atomic ordering and hardness of non-stoichiometric titanium carbide, Int. J. Refract. Met. HARD Mater. 15 (1997) 61–64, http://dx.doi.org/10.1016/S0263-4368(96)00020-0.

[50] P.A. Flinn, G.M. McManus, J.A. Rayne, Elastic constants of ordered and disordered Cu_3Au from 4.2 to 300° K, J. Phys. Chem. Solids 15 (1960) 189–195, http://dx.doi.org/10.1016/0022-3697(60)90242-0.

[51] G.-S. Wang, E.K. Delczeg-Czirjak, Q.-M. Hu, K. Kokko, B. Johansson, L. Vitos, The effect of long-range order on the elastic properties of Cu_3Au, J. Phys. Condens. Matter 25 (2013) 85401, http://dx.doi.org/10.1088/0953-8984/25/8/085401.

[52] A.P. Zhilyaev, T.R. McNelley, T.G. Langdon, Evolution of microstructure and microtexture in fcc metals during high-pressure torsion, J. Mater. Sci. 42 (2007) 1517–1528, http://dx.doi.org/10.1007/s10853-006-0628-0.

[53] D. Orlov, P.P. Bhattacharjee, Y. Todaka, M. Umemoto, N. Tsuji, Texture evolution in pure aluminum subjected to monotonous and reversal straining in high-pressure torsion, Scr. Mater. 60 (2009) 893–896, http://dx.doi.org/10.1016/j.scriptamat.2009.02.004.

[54] H.J. Bunge, R. Ebert, F. Günther, On the angular variation and texture dependence of Young's modulus in cold-rolled copper sheet, Phys. Status Solidi 31 (1969) 565–569, http://dx.doi.org/10.1002/pssb.19690310216.

[55] S.R. Claves, W.J. Mills, Influence of crystallographic texture on Young's modulus of various alloy 82H welds, Microsc. Microanal. 17 (2011) 341–349, http://dx.doi.org/10.1017/S1431927611000079.

[56] K. Edalati, Y. Ito, K. Suehiro, Z. Horita, Softening of high purity aluminum and copper processed by high pressure torsion, Int. J. Mater. Res. 100 (2009) 1668–1673, http://dx.doi.org/10.3139/146.110231.

[57] A.A. Mazilkin, B.B. Straumal, M.V. Borodachenkova, R.Z. Valiev, O.A. Kogtenkova, B. Baretzky, Gradual softening of Al-Zn alloys during high-pressure torsion, Mater. Lett. 84 (2012) 63–65, http://dx.doi.org/10.1016/j.matlet.2012.06.026.